Available online at www.sciencedirect.com

SciVerse ScienceDirect

Energy Procedia 37 (2013) 1448 – 1461

Energy Procedia

GHGT-11

Fireside corrosion of applied and modern superheater-alloys under oxy-fuel conditions

Gosia Stein-Brzozowska*, Jörg Maier, Prof. Günter Scheffknecht [a]

Danila Cumbo, Silvia Masci, Enrico Tosi [b]

Giovanni Corraggio, Marco Faleni, Leonardo Biasci [c]

[a] *Institute of Combustion and Power Plant Technology (IFK), University of Stuttgart, Germany*
[b] *Enel Engineering and Research, Via Andrea Pisano 120, Pisa, Italy*
[c] *International Flame Research Foundation (IFRF), Via Salvatore Orlando 5, 57123 Livorno, Italy*

Abstract

Operation of oxy-fuel power plants under ultra-supercritical parameters would help to overcome, to a certain extent, efficiency penalties from air separation and CO_2-compression units. To improve the knowledge on material behavior under oxy-fuel combustion six candidate superheater alloys, varying from martensitic via iron-base austenitic to nickel-base were chosen and exposed at metal temperature of 580°C and 650°C to real oxy-fuel combustion conditions in 3MW combustion test rig of Enel and subsequently moved for further tests to laboratory corrosion test set-up at IFK. Exact definition of combustion conditions was based on measurements performed by IFRF.

Selection and/or peer-review under responsibility of GHGT

Keywords: oxy-fuel; fireside corrosion; ultra-supercritical;

1. Introduction

Oxy-fuel combustion process including flue gas recirculation (FGR) was suggested in the early eighties for two purposes: to produce CO_2 for Enhanced Oil Recovery (EOR) by Abraham et al. [1] and/or to reduce environmental impacts in energy generation from fossil fuels by lowering significantly emitted CO_2, proposed by Horn and Steinberg [2].

In the nineties, due to the re-emerging discussions about how to prevent global warming, oxy-fuel combustion received renewed interest [3] and it has been seen as one of the most promising technologies

* Corresponding author. Tel.: +49 711 685 67762; fax: +49 711 685 63491
E-mail address: stein-brzozowska@ifk.uni-stuttgart.de OR maier@ifk.uni-stuttgart.de

1876-6102
Selection and/or peer-review under responsibility of GHGT
doi:10.1016/j.egypro.2013.06.020

for carbon capture and storage (CCS) [4] being economically and technically feasible for power station retrofitting [5]. Due to incorporation of processes demanding significant energy consumption (air separation unit and carbon dioxide purification and liquefaction units) the net plant efficiency operated in oxy-fuel mode would be by ca. 8-12% points lower compared to a conventional air fired power plant [6]. One of the solutions to reduce the efficiency penalty is raising the steam parameters. Therefore the information on the corrosive behavior of heat exchangers at the above mentioned conditions is of special interest at the Institute of Combustion and Power Plant Technology, University of Stuttgart, IFK and Enel Engineering and Research.

From the fireside, beside increased thermo-mechanical stresses, boiler materials need to face as well fouling, slagging and the gas atmosphere itself. Both fouling and slagging depend on the fuel quality and might be affected by increased metal surface temperature and different gas composition than in conventional air combustion. In conventional air-fired pulverized coal boilers applied widely in the energy sector air is supplied for oxidation purposes, whereas in an oxy-fuel combustor it is a blend of almost pure oxygen (> 95% oxygen purity) and recirculated flue gases. Since the dilution effect of nitrogen (79%-vol. of air) is missing in oxy-fuel compared to the conventional combustion of coal with air as an oxidizer much higher concentrations of CO_2, SO_2, H_2O, HCl, etc. are witnessed in oxy-fuel [6].

There is no sufficient data on corrosive performance neither of higher alloyed austenitic iron-base alloys, nor of nickel-base superalloys neither in conventional air nor under oxy-fuel coal combustion. Majority of studies have been performed on ferritic and martensitic alloys and often in a pure gas atmosphere without a deposit. Although very different conditions were applied in the reviewed tests some observations were repeating. The authors agree that water plays a significant role in oxide formation and its stability [7] - [11]. In certain cases the authors inform about poor protective quality of the oxides formed in oxy-fuel atmosphere [10]. Piron-Abellan [7] sees more protective chromium-rich surface scales formed during air exposure and buckling of outer hematite layer during tests in water rich environments. In case of some tested nickel and austenitic superalloys Natesan indicates that steam exacerbates the spallation of oxide scales on these alloys and leads to continued oxidation [10]. Increased oxidation of certain nickel superalloys in oxy-fuel combustion atmospheres compared to air combustion conditions were communicated by IFK before [11].

With increasing SO_2, oxygen and water concentrations, higher SO_2 to SO_3 conversion rates are expected [12], [13]. SO_3 is more reactive than SO_2 what might enhance sulfur induced corrosion due to formation of low melting eutectics like alkali-iron-trisulphates or Ni-Ni_3S_2 and Mo-Mo_2S_3, leading to an accelerated material loss.

The higher concentration of SO_3 promotes the sulfur retention in the ash at the convective section of the furnace (sulfur retention is negligible in radiative section, above 1150°C) [15]; this increased retention can intensify corrosion process from molten and solid ash in boiler deposits [5]. Significant issue influencing fireside corrosion is the deposit quality which might cause and/or accelerate sulfur-induced corrosion if high amount of alkalis like K and Na are present [16]; or impede it if fly ash acts as sulfur sink while forming stable minerals with sulfur [17].

Majority of the studies run on corrosion are performed in laboratory set-ups due to cost issues. In such tests flat metal coupons are used. Within this study metal samples in the form of rings cut from original boiler tubes were first exposed with a corrosion probe of University of Stuttgart in the combustion chamber of Enel's 3 MW combustion test rig thus being exposed to the real combustion conditions (atmosphere, fly ash deposit) and temperature gradient between the combustion gases and cooling medium. Moreover due to application of rings cut from metal tubes the samples witnessed real surface stresses. Six different alloys, varying from martensitic via austenitic to a nickel-based material were exposed at metal temperature of 580°C and 650°C. The samples were moved subsequently for the long term tests to the laboratory corrosion test set-up at the University of Stuttgart. Based on gas measurements

performed by IFRF it was possible to define exact combustion conditions and repeat them in the long-term corrosion tests.

Nomenclature

an	at analysed onditions
FoSper	3 MWth combustion test rig of Enel, located in Livorno, Italy
IFK	Institute of Combustion and Power Plant Technology, University of Stuttgart
IFRF	International Flame Research Foundation
waf	water ash free conditions
wf	water free conditions

2. Experimental part

2.1. Tested materials

Main focus of the corrosion tests was on austenitic iron-base alloys with varying chromium content. These are: 153MA, 304L, 253MA and 310S (see Table 1). 153MA has a similar composition as grade 304, however its Si-content is ca. 3 times higher; designed this way to have an impact on the oxidation performance at elevated temperatures. 304 grade has already been applied in the superheater and reheater sections of some of the first USC-boilers. Due to its austenitic character 304L cannot be hardened by heat treatment. However, it can be hardened by cold working, thus the steel might be found in the power plant sector in the shot-peened condition. Moreover 304 is known for its excellent weldability by all standard fusion methods [18]. 253MA has a very similar composition to the well-known Sanicro25. However, Si-content of 253MA is much higher than the one of Sanicro25 in order to improve the oxidation behavior of the alloy at elevated temperatures. With 7 % more Cr than 304, grade 310 is known to be a “perfect chromia-former” even in cyclic conditions. The lower carbon content of 310S does reduce its high temperature strength compared to 310 still offering good resistance to thermal fatigue and cyclic heating. Alloy 310 is widely used where sulphur dioxide gas is encountered at elevated temperatures [19]. Additionally a martensitic alloy T92 and a nickel-base grade 617 were selected for fireside corrosion tests.

Table 1. Composition of the tested alloys.

Alloy	Unit	Cr	Ni	Fe	Other
617	%-m.	22,0	Bal. (54,7)	1,1	C (0,006), Si (0,09), Mn, P, S, Mo, Co, Al, Pb
310S	%-m.	25,3	19,1	Bal.	C (0,046), Si (0,059), Mn, P, S, Co, Cu, N, Nb
253MA	%-m.	21,0	11,1	Bal.	C (0,086), Si (1,6), Mn, P, S, Co, Cu, N, Nb, Ce
153MA	%-m.	18,5	9,2	Bal.	C (0,053), Si (1,16), Mn, P, S, Co, Cu, N, Nb, Ce
304L	%-m.	18,2	8,2	Bal.	C (0,022), Si (0,4), Mn, P, S, N
T92	%-m.	8,8	0,2	Bal.	C (0,1), Si (0,24), Mn, P, S, Mo, V, B, N, W, Cb

2.2. Tests at FoSper

The combustion tests were performed in FoSper, 3 MWth combustion test rig of Enel located in Italy. The facility was kept in operation for about 50 hours at approximately 1,8 MWth and 61% dry recycle rate. A sulfur rich bituminous coal from Palma Rejo was selected for the tests (see Table 2 and Table 3).

The gas atmosphere composition and temperature together with heat flux and fly ashes were analyzed carefully in order to describe the exposure conditions in a very detailed way. The temperature and gas composition profile was measured in port no. 10 and 14 (see Fig.1). The temperature was measured with the IFRF standard suction pyrometer. The gas composition was double proved with a gas analyzer and an FTIR.

Table 2. Sulfur rich bituminous coal composition

	Unit	Concentration
Immediate analysis		
Moisture 105°C	%-m., an	1,8
Volatile Matters	%-m., waf	42,0
Ash	%-m., wf	8,1
Fixed carbon	%-m., waf	58,0
Elementary analysis		
C	%-m., waf	84,00
H	%-m., waf	5,66
N	%-m., waf	1,41
S	%-m., waf	1,52
Cl	ppm, waf	303
F	ppm, waf	47
Heating values		
HCV	J/g	30996
LCV	J/g	29855

Table 3. Sulfur rich bituminous coal: main elements in ash

	Unit	Concentration
Al_2O_3	%-m.	18,18
CaO	%-m.	7,23
Fe_2O_3	%-m.	8,50
K_2O	%-m.	1,50
MgO	%-m.	4,50
MnO_2	%-m.	0,13
Na_2O	%-m.	0,49
P_2O_5	%-m.	0,12
SiO_2	%-m.	51,74
TiO_2	%-m.	0,81

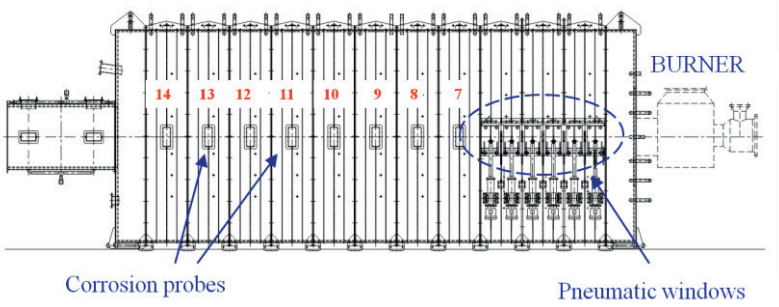

Fig.1. FoSper furnace drawing with the indications of the openings. Two corrosion probes were inserted in Port n°11 and Port n° 13. Temperature and gas composition were measured in Port 10 and 14.

Two corrosion probes were inserted inside the furnace, in windows no. 13 and 11 (see Fig.1 and Fig. 2). The dedicated samples temperatures were at approximately 580°C and 650°C in order to simulate the conditions for a supercritical and ultra-supercritical power plant in the super-heater and re-heater section of the combustion chamber.

After the successful exposure of the material rings with the corrosion probe of the University of Stuttgart, fireside corrosion was studied on every second ring directly in the laboratories of Enel and the remaining rings were carefully transported for further long-term corrosion tests to the laboratories of IFK.

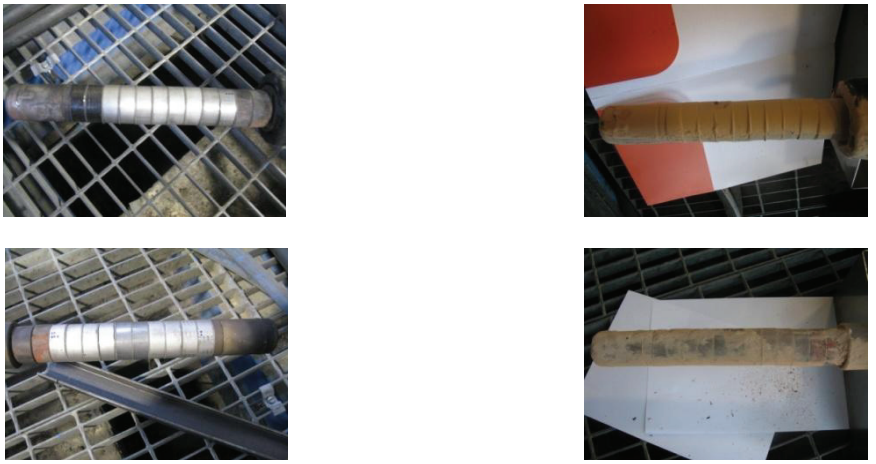

Fig. 2. Corrosion probes of IFK before (on the left) and after (on the right) the exposure in the combustion chamber of FoSper test rig of Enel in November 2011 during the tests with sulphur-rich coal.

2.3. Laboratory tests

The strategy of IFK is to expose materials in a real combustor like FoSper facility until the first oxide scale and an initial fly ash deposition layer are formed. The rings are further moved to the laboratory corrosion test set-up of IFK for the long term corrosion tests (up to 1000 h).

The corrosion test set-up consists of electrically heated furnaces supplied with a gas blend which can be composed of water vapor, CO_2, O_2, SO_2 and N_2 and adjusted easily according to the needs of the given experiment [20]. The dedicated samples temperatures correspond to samples temperatures as exposed in the combustion chamber of FoSper at 580°C and 650°C. The gas blend (Table 4) was adjusted in order to enable a comparison of the current studies with similar ones performed with sulfur-lean bituminous coal deposits [21].

Table 4. Gas compositions for the long term high temperature corrosion tests

	Temperature [°C]	O_2 [%-vol.]	CO_2 [%-vol.]	H_2O [%-vol.]	SO_2 [%-vol.]
Series 1	580°C	3	86	11	0.3
Series 2	650°C	3	86	11	0.3

2.4. Analytics

After the exposure tests samples were cooled and subsequently carefully embedded in a resin. Following grinding and polishing of the samples surfaces, the analyses were performed. Standard reflected light microscopy techniques were applied for the first characterization. For more detailed investigation of the reaction processes, electron microscopy techniques were applied. The two-dimensional distribution of chemical elements was investigated [20] [22]. In certain cases part of the deposit was removed without affecting the analyzed metal surface and further ICP and XRD analyses were performed whenever possible [17].

3. Results and discussion

3.1. Combustion atmosphere

The average gas composition was as follows: 64,2%-vol. CO_2, 3,7%-vol. O_2, 20,3%-vol. N_2 and 11,8%-vol. H_2O. Even though the plant was kept in operation at stable conditions during the whole period, the temperature and gas composition inside the furnace was measured daily in the both windows (10 and 14). Only slight differences were observed in the temperature and gas composition during the three days of operation. The temperature profile was quite flat in both windows due to the distance from the burner; in window n°10 the average temperature was always about 100°C higher than the average temperature in window n°14 (see **Error! Reference source not found.**). This behavior is expected because the furnace is cooled and, at the distance of port n°10, the great part of the combustion heat is already released, therefore, starting from that point, the temperature of the flue gas started to decrease. Nevertheless the oxidation is still proceeding as demonstrated by the concentration of carbon monoxide that is ten times greater in port n°10 compared to the values in port n°14. At the same time CO_2 and H_2O concentrations are higher at the end of the furnace than in port n°10 and opposite happens to the oxygen concentration. In **Error! Reference source not found.** the SO_2 profile measured during the second day of operation is shown. In order to demonstrate the accuracy of the performed SO_2 measurements two analytical instruments were used simultaneously: NDIR and FTIR. One important result of the performed measurements is the very good agreement between SO_2-concentrations obtained by the both analyzers. The medium values of the other chemical compounds are shown in Table 5 and Table 6.

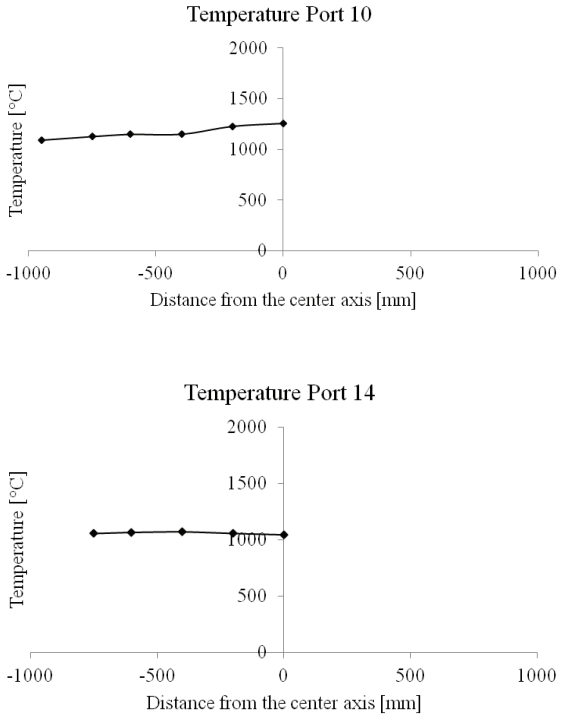

Fig. 3. Temperature profile in ports 10 and 14 during the second day of operation

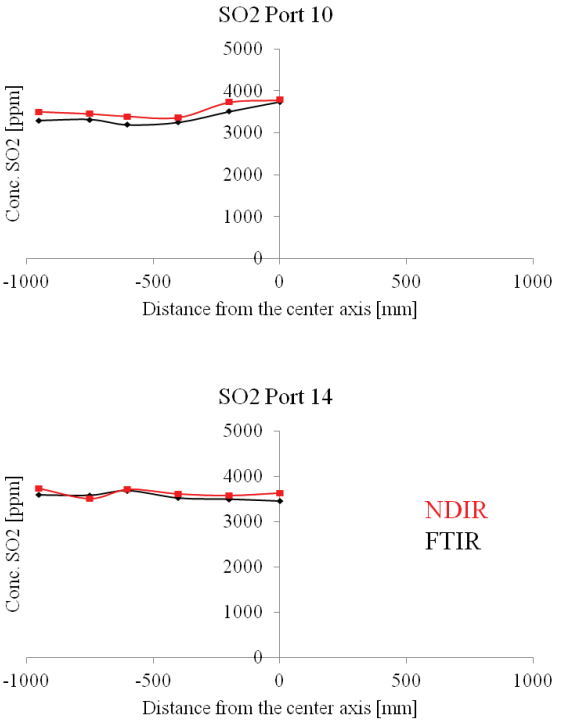

Fig. 4. Sulfur dioxide concentration, dry in Port 10 and 14 during the second day of operation and with two parallel analyzers

Table 5. Temperature and gas composition in port 10; average values during the 3-day-operation

Temp [°C]	O_2 [%-vol.]	CO_2 [%-vol.]	H_2O [% vol.]	CO [vppm]	NO [vppm]	SO_2 [vppm]	N_2 [%-vol.] (by difference)
1119	9,2	61,6	10,8	844	232	2896	18

Table 6. Temperature and gas composition in port 14; average values during the 3-day-operation

Temp [°C]	O_2 [%-vol.]	CO_2 [%-vol.]	H_2O [% vol.]	CO [vppm]	NO [vppm]	SO_2 [vppm]	N_2 [%-vol.] (by difference)
969	6	63,5	11,9	83	201	3096	18,2

3.2. Deposit

The primary deposit layer collected from the rings exposed in combustion test rig reveals much higher sulphur contents compared to other collected fly ashes (Fig. 5). Although the earth alkali content is low, calcium magnesium sulphate is often detected on the cooled surfaces. Similar is encountered during the tests with sulphur-lean bituminous coal [23] and lignite [24].

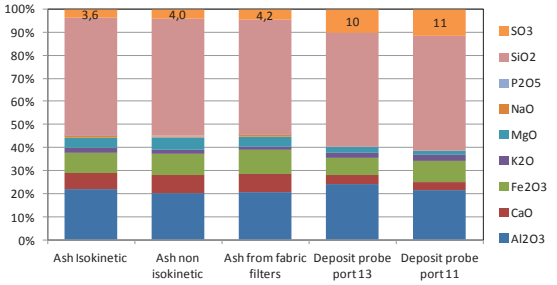

Fig. 5. Composition of fly ashes and fly ash deposits collected during combustion tests with S-rich bituminous coal at FoSper.

During the laboratory exposures new fly ash layer was added after the first 350 h and repeated every 200 h in order to simulate deposition of fresh fly ash on heat exchangers within boiler. The analysis of fly ash deposit performed after the laboratory tests had been completed, reveals enrichment with sulfur over time by more than factor four, what indicates the sulphur-binding capacity of fly ash and thus its partly protective role in sulfur-induced fireside corrosion.

3.3. Fireside corrosion

Significant during fireside corrosion tests in terms of material is not only its composition but also surface quality. In the presented study original tube surfaces of all the six examined materials were used. Important to add is the fact that the four iron-base austenites were longitudinally welded tubes provided by Outokumpu[†].

The formed oxide scales vary widely in character among the studied materials and approaches already after 50 h from nanometers-range in case of a nickel-base alloy up to few micrometers in case of a martensitic alloy. After 950 h more, chromium-rich oxides reach up to 5 µm at nickel superalloy and more than double as much on T92 at 580°C and on lower chromium austenites at 650°C.

The martensitic alloy T92, exposed only at 580°C, shows much bigger oxide scale than the tested austenites. Already after 50 h of testing in the test rig 10 µm chromium rich internal oxide is observed and ca. 20 µm external oxide growing into fly ash is witnessed. After 1000 h exposure (see Fig. 6) the values reach ca. 15 µm and 22 µm, respectively. Additionally a mixed chromium iron oxide (ca. 25 µm)

[†] Longitudinally welded tubes provide a cost-efficient alternative to the seamless tubes traditionally used in for e.g. superheaters in power generation. If NDT is performed according to EN 10217-7 then this allows a design strength utilisation of 100% and a weld factor Z = 1.0 for pressure calculation under EN 13480-3. This means that the welded tube is considered to have the same strength as a seamless tube for design purposes. Sources: Dr. Rachel Pettersson, Outokumpu and Elin M. Westin, David Garrett, Asko Kähönen, Hans Storbacka and Sören Nytomt: Welded stainless steel tubes & pipes vs. seamless. Paper presented at INOX 2010, Brazil

sandwiched between internal oxide and hematite layer is observed, however presence of chromite is not confirmed with point analyses.

Generally with increasing chromium content of the alloy, also a better metal performance is expected [17] [25] [26]. However in this study not only the chromium content seems to be playing an important role in metal loss. Although at 580°C metal temperature similar material loss has been observed among tested austenites (7-10 μm), with increasing temperature (650°C metal temperature) differences in corrosion rate among tested austenitic grades become more obvious and are in the range 10 – 25 μm.

Alloy 153MA characterized by much lower chromium content than grade 310S (18,5% vs. 25,3%) displays a slightly better corrosion rate. The character and morphology of corrosion products vary significantly between the two grades (see

Fig. 9. Total maximum corrosion product [μm] concerning the form after exposures with Palma Rejo fly ash at 580°C after 1000h.

Fig. 10. Total maximum corrosion product [μm] concerning the form after exposures with Palma Rejo fly ash at 650°C after 1000h.

). Alloy 304L though having a chromium content very similar to that of alloy 153MA (18,2% vs. 18,5%), displays higher corrosion rates (up to ca. 26 μm after 1000 h at 650°C). The best performance at the studied conditions is revealed by alloy 253MA (21% Cr) with metal loss at ca. 10 μm after 1000 h at 650°C, which is also characterized by a lower chromium content than grade 310S (25,3%). A deeper corrosion attack is noticed on alloy 310S due to the presence of pits along the whole surface that appear to grow with time indicating a possibility of intergranular corrosion. These pits might be the effect of pickling which the alloy underwent during the pre-processing. Whereas alloy 310S displays thin regular pits, alloy 253MA shows broad pits leading to a through shaped corrosion front.

Alloy 153MA showing a very irregular corrosion front performs slightly better than 304L also characterized by an irregular corrosion front (Fig. 8). Grade 153MA, similarly as 253MA, is alloyed with higher silicon content compared with other tested materials. As mentioned before with increased silicon content steel manufacturer wanted to provide the alloys with higher corrosion resistance at elevated temperatures. Interesting is the buckling effect of oxide scale leading to its spallation on alloy 304L at 580°C however not observed at 650°C.

Oxidation, as expected, increases with temperature, however none of the tested alloys manages to develop a continuous compact chromia scale within 1000 h although strings of chromia are often noticed along the surfaces of austenites.

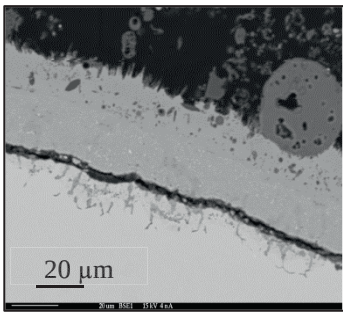

Fig. 6. T92, 580°C after 50 h exposure in Fosper and further 950 h in corrosion test set-up at IFK

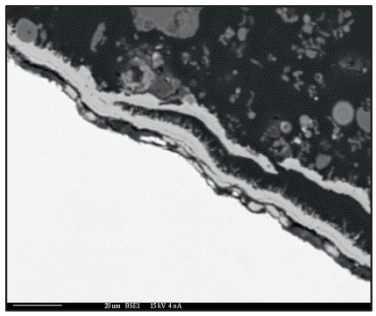

Fig. 7. 304L 580°C after 50 h exposure in Fosper and further 950 h in corrosion test set-up at IFK

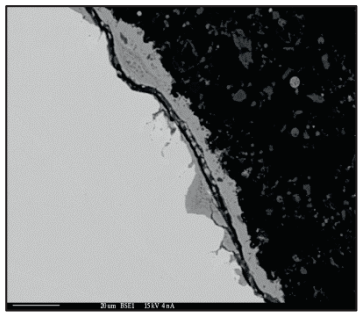

Fig. 8. 304L 650°C after 50 h exposure in Fosper and further 950 h in corrosion test set-up at IFK

At 580°C on two of the alloys (T92 and 304L) whiskers are detected (Fig. 6 and Fig. 7). Formation and volatilization of $Fe(OH)_2$ might account to accelerated oxidation rates of steels in the presence of water vapor [27]. Moreover after Astermann [28] H_2O vapor containing atmospheres have a detrimental effect at T>600°C in austenitic steels due to Cr-evaporation.

Tested nickel superalloy developes quickly a protective chromia layer similar at both temperatures. Also independently of the temperature an intergranular oxidation accompanied by aluminum oxide is noticed going as far as 22 µm at 580°C and 26 µm at 650°C. At certain areas aluminum seems to diffuse outwards leaving a depletion zone behind. Locally sulfur presence was noticed in reaction with Cr_2O_3.

A detailed information on distribution of the oxides is presented in

Fig. 9. Total maximum corrosion product [µm] concerning the form after exposures with Palma Rejo fly ash at 580°C after 1000h.

Fig. 10. Total maximum corrosion product [µm] concerning the form after exposures with Palma Rejo fly ash at 650°C after 1000h.

und Fig. 10.

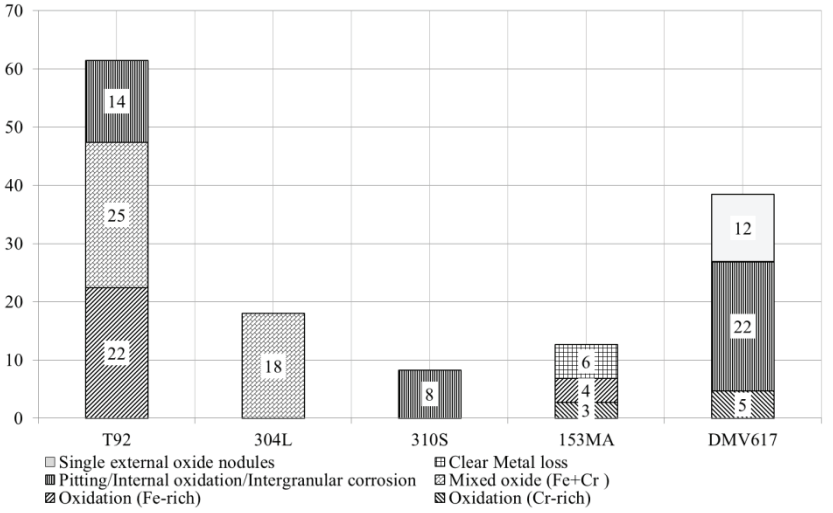

Fig. 9. Total maximum corrosion product [μm] concerning the form after exposures with Palma Rejo fly ash at 580°C after 1000h.

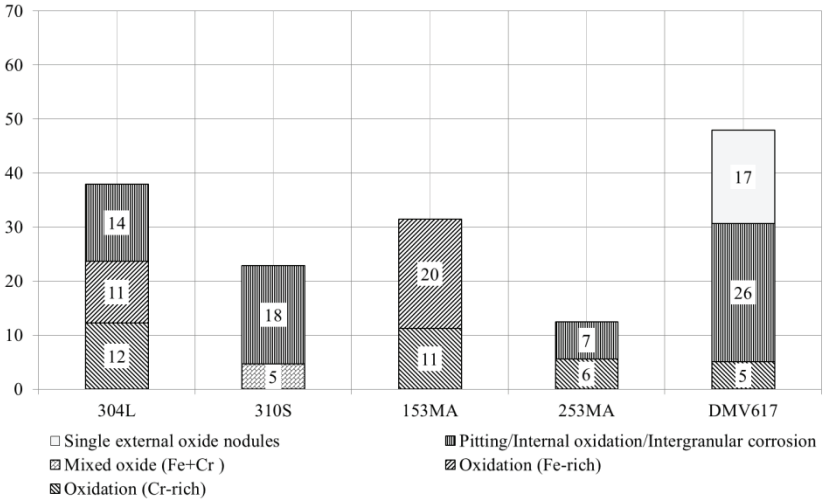

Fig. 10. Total maximum corrosion product [μm] concerning the form after exposures with Palma Rejo fly ash at 650°C after 1000h.

4. Conclusions

Within the first 50 h in the boiler of the FoSper test rig a uniform layer of fine adhesive fly ash particles builds the initial deposition layer during combustion of Palma Rejo bituminous coal. The fly ashes building the initial deposition layer tend to bind sulphur more effectively than any other collected

fly ashes. Henceforth, especially in case of higher SO_2 concentrations in oxy-fuel this effect might pose a significant threat in case of sulphur rich coals with high potassium and sodium contents. The fly ashes creating the initial deposition layer contain approximately three times more sulphur than corresponding secondary layers, what confirms earlier observations of IFK during the combustion tests with different lignite qualities.

In terms of fireside corrosion the critical issue is the stability of newly-formed minerals binding sulphur and their tendency to form eutectics at temperatures similar to tubes temperature, therefore studies on mineral composition are run simultaneously with the examinations on corrosion products. In here performed study fly ashes did not exhibit any corrosive influence; on the contrary they seem to act as "sulfur sink" while capturing sulfur via earth alkalis.

As expected, higher corrosion rates are measured at higher temperature. Austenitic alloys witness a metal loss in the range 7 – 10 µm at 580°C metal temperature and perform much better than martensitic steel revealing corrosion rate in the range 30 – 40 µm after 1000 h at the same temperature. With increasing temperature (650°C metal temperature) differences in metal loss among the examined austenitic grades become more obvious and are in the range 10 – 25 µm.

Observing the behavior of austenitic alloys 304L, 153MA, 253MA and 310S a direct relation between chromium content and corrosion performance cannot be made. Grades 253MA (22,1% Cr) and 153MA (18,5% Cr) show the lowest metal loss with ca. 10 µm and 15 µm after 1000 h at 650°C, respectively and are followed by 310S (25,3% Cr) displaying a metal loss of ca. 20 µm at the same conditions. The corrosion morphologies vary significantly. T92 witnesses internal corrosion increasing with time, whereas alloy 304L displays some buckling and spalling at lower exposure temperature. Both alloys form a thick mixed oxide layer at 580°C (304L up to 18 µm and T92 up to 25 µm). Occasionally whiskers are noticed at 580°C at T92 and at 304L. Their effect on long-term performance of alloy should be a topic of further studies. Nickel superalloy oxidizes slowly showing barely any signs of corrosion attack at the surface, however occasionally intergranular oxidation accompanied by aluminum oxide reaching up to ca. 30 µm is noticed.

Acknowledgements

The authors are very grateful to the EU since the above described work was performed in the frame of the OxyCorr Project which was partly funded by the RFCS Research Program of the European Commission (RFCR-CT-2009-00005). More information about OxyCorr is available on http://oxycorr.eu-projects.de/

Moreover, the authors would like to express our gratitude to Dr. Rachel Pettersson from Outokumpu for her great effort in provision of tubes and to Mr. Matthias Pagano from IFK-KWF for supporting the measuring campaign and to all the unnamed employees of Enel and IFRF for their contribution to the successful operation of FoSper test rig.

References

[1] Abraham BM, Asbury JG, Lynch EP, Teotia APS. Coal-oxygen process provides CO2 for enhanced recovery. Oil Gas J 1982; 80 (11): 68-70.

[2] Horn FL, Steinberg M. Control of carbon dioxide emissions from a power plant (and use in enhanced oil recovery). Fuel 1982; 61(5): 415 – 22.

[3] Tan R, Corragio G, Santos S. Oxy-coal combustion with flue gas recycle for the power generation industry - a literature review. Study report, IFRF Doc. No. G23/y/1. Velsen-Noord, The Netherlands: International Flame Research Foundation (IFRF); September 2005.
[4] Toftegaard M, Brix J, Jensen P. Oxy-fuel combustion of solid fuels. Progress in energy and combustion science 2010; 36: 581 - 625.
[5] Stanger R, Wall T. Sulphur impacts during pulverised coal combustion in oxy-fuel technology for carbon capture and storage. Progress in Energy and Combustion Science 2011; 37: 69 – 88.
[6] Scheffknecht G, Al-Makhadmeh L, Schnell U, Maier J. Oxy-fuel coal combustion – A review of the current state-of-the-art. International Journal of Greenhouse Gas Control. Volume 5, Supplement 1, Oxyfuel Combustion Technology - Working Toward Demonstration and Commercialisation, July 2011, pages: S16-S35, ISSN 1750-5836; DOI:10.1016/j.ijggc.2011.05.020; 2011
[7] Piron-Abellan J, Olszewski T, Meier GH, Singheiser L, Quadakkers WJ. The oxidation behaviour of the 9% Cr-steel P92 in CO2- and H2O-rich gases relevant to oxy-fuel environments. International Journal of Materials Research. 2010: 287-299.
[8] Huenert D, Schulz W, Kranzmann A. Corrosion of steels in H2O-CO2 atmospheres at temperatures between 500°C and 700°C Federal Institute of Materials Research and Testing, Berlin; September 8–11, 2008. P R E P R I N T – ICPWS XV.
[9] Montgomery M, Hjörnhede A, Gerhardt A. Short-term corrosion testing in a burner rig with oxy-fuel and conventional firing. Nice, France; September 6 – 10, 2009; 5-20.
[10] Natesan K, Rink DL, Zeng Z. Materials performance of structural alloys in simulated oxy-fuel environments. 24th Annual Conference on Fossil Energy Materials. Pittsburgh, USA; May 25-27, 2010.
[11] Stein-Brzozowska G, Maier J, Scheffknecht G. Deposition Behavior and Superheater Corrosion under Coal Fired Oxyfuel Conditions, Special Workshop on Oxyfuel Combustion Addressing SO2/SO3/Hg and Corrosion Issues. London, Jan. 25-26, 2011.
[12] Mönckert P, Dhungel B, Kull R, Maier J. Impact of combustion conditions on emission formation (SO2, NOx) and fly ash. 3rd workshop of the IEA GHG international oxy-combustion network. Yokohama, Japan; March 5-6, 2008.
[13] Klostermann M. Efficiency increase of the oxyfuel process by waste heat recovery considering the effects of flue gas treatment. 3rd workshop of the IEA GHG international oxy-combustion network. Yokohama, Japan; March 5 - 6, 2008.
[14] Spörl R, Maier J, Scheffknecht G. Experiences and results of SO3 measurements performed under oxy-coal fired conditions. Special workshop on oxy-fuel combustion: addressing SO2/SO3/Hg and corrosion issues. London, England; Jan. 25-26, 2011.
[15] Scheffknecht G, Maier J. Firing issues related to the oxy-fuel process. VGB Power Tech. 2008; 11: 91-97.
[16] Maier J, Stein-Brzozowska G., Lemp O, Babat S, Neuwirth A, Schnell U, Scheffknecht G . Verbundprojekt COORETEC DE1: Korrosion und Verschlackung in Hochtemperaturkraftwerken mit neuen Werkstoffen, Teilvorhaben: Grundlegende experimentelle Untersuchungen zur Korrosion und Belagsbildung an neuen Werkstoffen für den Einsatz in Hochtemperaturkraftwerken sowie Erweiterung von Modellen im Zusammenhang mit der Gesamtprozessbetrachtung; Abschlussbericht; Universität Stuttgart Institut für Feuerungs- und Kraftwerkstechnik; Stuttgart 2011
[17] Stein-Brzozowska G, Flórez DM, Maier J, Scheffknecht G. Fireside Corrosion of Dedicated Austenitic Steels in Ultra-Supercritical Coal-Fired Power Plants, THE 37TH INTERNATIONAL TECHNICAL CONFERENCE ON CLEAN COAL AND FUEL SYSTEMS. Clearwater, USA; June 3-7, 2012. article in press, APEN-D-12-01927.
[18] http://www.outokumpu.com/35046.epibrw
[19] http://www.azom.com/article.aspx?ArticleID=966
[20] Stein-Brzozowska G, Miller E, Kull R, Maier J, Scheffknecht G. Vergleich der am IVD untersuchten Vorgehensweisen zur Bestimmung der Korrosionsmechanismen an ausgewählten Überhitzerwerkstoffen unter Oxyfuel-Bedingungen, Conference book „Kraftwerkstechnik sichere und nachhaltige Energieversorgung“ by Beckmann M., Hurtado A., 41. KraftwerktstechnischesKolloquium. Dresden, Germany, October 13.-14, 2009.
[21] 2ndOxyfuel Combustion Conference,Influence of oxy-coal on corrosion behavior of the chosen heat-exchanger materials,Danila Cumboa, Gosia Stein-Brzozowska, Eva Miller, Jörg Maier, Prof. G. Scheffknechtb, Peter Viklundc
[22] Stein-Brzozowska G., Maier J., Scheffknecht G.: Impact of the Oxy-Fuel Combustion on the Corrosion Behavior of the Chosen Super-Heater Materials, 10th International Conference on Greenhouse Gas Control Technologies, 19th-23rd September 2010, RAI, Amsterdam, The Netherlands, Energy ProcediaVolume 4, 2011, Pages 2035–2042
[23] Cumbo D, Stein-Brzozowska G, Miller E, Maier J, Scheffknecht G, Viklund P. Influence of oxy-coal on corrosion behavior of the chosen heat-exchanger materials. 2ndOxyfuel Combustion Conference. Queensland, Australia, September 12-16 2011.
[24] Stein-Brzozowska G, Babat S, Maier J, Scheffknecht G. Influence of oxy-coal on fly ash transformations and corrosion behavior of heat-exchangers. 2ndOxyfuel Combustion Conference. Queensland, Australia, September 12-16 2011.
[25] Khanna A.S. Introduction to high temperature oxidation and corrosion. 1st edition, ASM International; 2002, ISBN: 0-87170-762-4.

[26] Gagliano MS, Hack H, Stanko G. Fireside Corrosion Resistance of Proposed USC Superheater and Reheater Materials: Laboratory and Field Test Results. The 33th International Technical Conference on Coal Utilization & Fuel Systems, June 1 – 5, 2008, Clearwater, FL, USA

[27] Surman PL, Castle JE. Gas phase transport in the oxidation of Fe and steel. Corrosion Science. Volume 9, Issue 10, 1969, Pages 771–772, IN1–IN2, 773–777

[28] Asteman. H, Svensson J, Johansson LG. Effect of Water-Vapor-Induced Cr Vaporization on the Oxidation of Austenitic Stainless Steels at 700 and 900°C. Journal of electrochemical society. 151 (3) (2004), 141-150.